

# The origins of off-centre massive black holes in dwarf galaxies

Jillian M. Bellovary<sup>1</sup>,<sup>1,2,3</sup>★ Sarra Hayoune,<sup>4</sup>★ Katheryn Chafra,<sup>5</sup> Donovan Vincent,<sup>6</sup> Alyson Brooks,<sup>7</sup>★ Charlotte R. Christensen,<sup>8</sup> Ferah D. Munshi,<sup>9</sup> Michael Tremmel,<sup>10</sup> Thomas R. Quinn,<sup>11</sup> Jordan Van Nest,<sup>9</sup> Serena K. Sligh<sup>9</sup> and Michelle Luzuriaga<sup>12</sup>

<sup>1</sup>Department of Physics, Queensborough Community College, City University of New York, 222-05 56th Ave, Bayside, NY 11364, USA

<sup>2</sup>Department of Astrophysics, American Museum of Natural History, Central Park West at 79th Street, New York, NY 10024, USA

<sup>3</sup>Department of Physics, Graduate Center, City University of New York, New York, NY 10016, USA

<sup>4</sup>Department of Physics, Stevens Institute of Technology, Hoboken, NJ 07030, USA

<sup>5</sup>University of Connecticut, School of Engineering, Storrs, CT 06269, USA

<sup>6</sup>Manhattan College, Riverdale, NY 10471, USA

<sup>7</sup>Department of Physics & Astronomy, Rutgers University, 136 Frelinghuysen Road, Piscataway, NJ 08854, USA

<sup>8</sup>Department of Physics, Grinnell College, 1115 8th Ave, Grinnell, IA 50112, USA

<sup>9</sup>Department of Physics and Astronomy, University of Oklahoma, 440 W. Brooks St, Norman, OK 73019, USA

<sup>10</sup>Department of Astronomy, Yale University, 52 Hillhouse Ave, New Haven, CT 06511, USA

<sup>11</sup>Department of Astronomy, University of Washington, Box 351580, Seattle, WA 98122, USA

<sup>12</sup>Queens College, City University of New York, Queens, NY 11367, USA

Accepted 2021 June 7. Received 2021 May 13; in original form 2021 February 14

## ABSTRACT

Massive black holes often exist within dwarf galaxies, and both simulations and observations have shown that a substantial fraction of these may be off-centre with respect to their hosts. We trace the evolution of off-centre massive black holes (MBHs) in dwarf galaxies using cosmological hydrodynamical simulations, and show that the reason for off-centre locations is mainly due to galaxy–galaxy mergers. We calculate dynamical time-scales and show that off-centre MBHs are unlikely to sink to their galaxies’ centres within a Hubble time, due to the shape of the hosts’ potential wells and low stellar densities. These wandering MBHs are unlikely to be detected electromagnetically, nor is there a measurable dynamical effect on the galaxy’s stellar population. We conclude that off-centre MBHs may be common in dwarfs, especially if the mass of the MBH is small or the stellar mass of the host galaxy is large. However, detecting them is extremely challenging, because their accretion luminosities are very low and they do not measurably alter the dynamics of their host galaxies.

**Key words:** black hole physics – galaxies: dwarf – software: simulations.

## 1 INTRODUCTION

Observational evidence has been mounting for the existence of massive black holes (MBHs) in dwarf galaxies, which inform our understanding of MBH–host galaxy scaling relations as well as provide clues to the origins of supermassive black hole (SMBH) seeds. These MBH candidates have been discovered in several ways, including via X-rays (Pardo et al. 2016; Baldassare et al. 2017; Mezcua et al. 2018; Birchall, Watson & Aird 2020), broad and narrow emission lines (Reines, Greene & Geha 2013; Moran et al. 2014; Chilingarian et al. 2018; Dickey et al. 2019; Cann et al. 2020), infrared emission (Satyapal et al. 2014), nuclear variability (Baldassare, Geha & Greene 2018; Martínez-Palomera et al. 2020), radio emission (Mezcua, Suh & Civano 2019; Reines et al. 2020), and masers (Zaw et al. 2020). As the number of candidates increases, one can begin to compile a sample and determine whether overall these lower mass counterparts of massive galaxies fall on the same scaling

relations, such as  $M_{\text{BH}} - \sigma$ ,  $M_{\text{BH}} - M_{\text{bulge}}$ , and  $M_{\text{BH}} - M_{\text{star}}$ . While some efforts portend that the  $M_{\text{BH}} - \sigma$  relation does not change as masses decrease (Baldassare et al. 2020), others find evidence of a low-mass downturn of the  $M_{\text{BH}} - M_{\text{bulge}}$  relation (Graham & Scott 2015; Mezcua 2017). See Greene, Strader & Ho (2020) for a thorough review on this topic.

MBHs in dwarf galaxies are not always straightforward to detect, however. In our prior work, Bellovary et al. (2019) found that approximately half of MBHs in simulated dwarf galaxies are not located in the nuclear regions of their galaxies. This result was confirmed observationally by Reines et al. (2020), who executed a radio survey of 111 dwarf galaxies detected in FIRST. Of their sample of dwarf galaxies with compact radio sources consistent with active galactic nucleus (AGN) activity, approximately half are off-centre. Mezcua & Domínguez Sánchez (2020) also show evidence for off-centre AGN activity in dwarfs, as indicated by spatially resolved emission lines.

Off-centre MBHs will have different dynamical and accretion histories than their nuclear counterparts, and will thus have different effects on their host galaxies. Since these MBHs spend a large fraction of their orbits in less dense regions, they will undergo fewer

\* E-mail: [jbellovary@amnh.org](mailto:jbellovary@amnh.org) (JMB); [sarah.hayoune@gmail.com](mailto:sarah.hayoune@gmail.com) (SH); [abrooks@physics.rutgers.edu](mailto:abrooks@physics.rutgers.edu) (AB)

accretion events. Thus, host galaxies may experience less quenching of star formation, because of the lack of radiation feedback due to accretion on to the black hole. The MBHs themselves will be more difficult to detect electromagnetically, since their accretion luminosities will be low. Gravitational waves from MBH–MBH mergers in dwarf galaxies will also be rare if one or more MBHs are off-centre; the odds of the black holes forming a bound pair are decreased.

These observational challenges have important repercussions. The difficulty of detecting these MBHs will result in an underestimate of the occupation fraction of MBHs in dwarf galaxies as well as the overall density of MBHs in the Universe. Since dwarf galaxies are the most numerous type of galaxy, this underestimate may be substantial. Statistical measurements of occupation fractions (as well as more direct measurements of black hole masses) are important because they can aid in constraining the formation mechanism(s) of SMBH seeds (Volonteri & Natarajan 2009; Greene 2012; Miller et al. 2015), as can gravitational wave measurements by future observatories such as the Laser Interferometer Space Antenna (LISA; Ricarte & Natarajan 2018). Most theoretical predictions of these quantities assume central MBHs, and contain corresponding assumptions about their detectability. It is thus imperative that we understand and quantify the off-centre fraction.

In this paper, we explore the origins and detectability of off-centre MBHs in dwarf galaxies. In Section 2, we describe the simulations used in our study. We examine how MBHs become off-centre in Section 3, and why they remain off-centre in Section 4. In Section 5, we will discuss whether off-centre MBHs can be detected, and we summarize our results in Section 6.

## 2 SIMULATIONS

We use the state-of-the-art  $N$ -body Tree + smoothed particle hydrodynamics (SPH) code ChaNGa (Menon et al. 2015) to simulate realistic dwarf galaxies. This code as well as its predecessor GASOLINE (Stadel 2001; Wadsley, Stadel & Quinn 2004) uses modern methods and realistic subgrid models to reproduce a range of observed galaxy properties using high-resolution simulations (Anderson et al. 2017; Munshi et al. 2017; Tremmel et al. 2018; Bellovary et al. 2019; Sanchez et al. 2019; Applebaum et al. 2020; Akins et al. 2021; Wright et al. 2021). The particular simulations in this work are known as the MARVEL-ous Dwarfs and the DC Justice League, and are described in detail in Bellovary et al. (2019); we summarize them here.

### 2.1 Simulation properties

All of our simulations use a modern SPH kernel calculation, which uses a geometric mean density in the SPH force expression and accurately reproduces shearing flows (Ritchie & Thomas 2001; Menon et al. 2015; Wadsley, Keller & Quinn 2017). They include a uniform ultraviolet background (Haardt & Madau 2012) and metal diffusion and cooling (Shen, Wadsley & Stinson 2010). Star formation is determined by the molecular gas fraction as described in Christensen et al. (2012). Stars form probabilistically when the gas density surpasses a threshold of  $\rho_{\text{th}} > 0.1 \text{ cm}^{-3}$ , although the actual density of star-forming gas is usually  $10\text{--}1000 \text{ cm}^{-3}$  due to the molecular gas requirement. In addition, the gas temperature must be  $T < 1000 \text{ K}$ . We set the star formation efficiency parameter equal to  $c_* = 0.1$ , and stars form with a Kroupa initial mass function (Kroupa 2001). Supernovae release  $E_{\text{SN}} = 1.5 \times 10^{51} \text{ erg}$  in accordance with the blastwave model described in Stinson et al. (2006), which disables

cooling for the theoretical lifetime of the momentum conserving phase.

Our simulations were selected from two different uniform volumes, using the ‘zoom-in’ technique (Katz & White 1993). The suite known as the ‘MARVEL-ous Dwarfs’ (Captain Marvel, Elektra, Rogue, and Storm; Munshi et al. 2021) was selected from a 25 Mpc volume, and has a force softening resolution of 60 pc and particle masses of  $M_{\text{dark}} = 6660 M_{\odot}$ ,  $M_{\text{gas}} = 1410 M_{\odot}$ , and  $M_{\text{star}} = 442 M_{\odot}$  (‘mint’ resolution as described in Applebaum et al. 2020). It uses a *WMAP3* cosmology (Spergel et al. 2007) and consists of 65 galaxies. The other suite, known as the ‘DC Justice League’ (Sandra, Ruth, Sonia, and Elena), was selected from a 50 Mpc volume, and has a force softening resolution of 170 pc and particle masses of  $M_{\text{dark}} = 4.2 \times 10^4 M_{\odot}$ ,  $M_{\text{gas}} = 2.7 \times 10^4 M_{\odot}$ , and  $M_{\text{star}} = 8000 M_{\odot}$  (‘near-mint’ resolution). It uses a *Planck* cosmology (Planck Collaboration I 2014) and consists of 113 dwarf galaxies. Dwarf galaxies are defined as having resolved star formation histories (star formation spanning more than 100 Myr), and minimum and maximum total masses of  $10^7$  and  $2.5 \times 10^{11} M_{\odot}$ , respectively. We identify galaxies using the Amiga Halo Finder (Gill, Knebe & Gibson 2004; Knollmann & Knebe 2009), which identifies haloes as spherical regions within which the density satisfies the redshift-dependent overdensity criterion approximated by Bryan & Norman (1998).

The two sets of simulations (MARVEL-ous Dwarfs and DC Justice League) differ in both their resolutions and the cosmologies used. Cosmology will have a minor effect compared to environmental factors on properties such as MBH and star formation, and we do not anticipate any issues due to the difference. All recipes for star formation, feedback, and black hole physics (including the seed mass) are the same, regardless of resolution. There are no systematic differences between the two data sets; dwarfs in both suites lie along the same observed scaling relations such as stellar mass–halo mass, size–luminosity, and mass–metallicity (Munshi et al. 2021).

### 2.2 Black hole physics

All black hole physics in our simulations is described in detail in Bellovary et al. (2019); here, we present a summary. Black hole particles form from collapsing, cool ( $T < 2 \times 10^4 \text{ K}$ ), low-metallicity ( $Z < 10^{-4}$ ) gas that has a low molecular gas content ( $f_{\text{H}_2} < 10^{-4}$ ). These criteria are meant to broadly represent the direct collapse scenario (e.g. Oh & Haiman 2002; Begelman, Volonteri & Rees 2006; Lodato & Natarajan 2006). The threshold density for black hole formation is  $3000 \text{ cm}^{-3}$  for the lower resolution runs, and  $1.5 \times 10^4 \text{ cm}^{-3}$  in the higher resolution simulations. The gas particle must also exceed a Jeans mass criterion, which ensures that the particle is in a region that is likely to collapse. Once formed, the MBH particle accretes mass from the surrounding gas, until it either depletes its neighbourhood (i.e. one softening length) of gas or reaches a mass of  $50\,000 M_{\odot}$ , whichever happens first. In some cases in the Justice League simulations, the neighbourhood is depleted first, resulting in black holes with masses of  $\sim 25\,000 M_{\odot}$ .

We do not resolve the scales at which MBH–MBH pairs coalesce and merge. When our particles form a close pair, which involves them having a separation far below our resolution limit, we treat them as a single particle. Specifically, they must have an interparticle distance of less than two softening lengths, and also meet the criterion  $\frac{1}{2} \Delta v < \Delta a \cdot \Delta r$ , where  $\Delta v$ ,  $\Delta a$ , and  $\Delta r$  represent the relative velocity, acceleration, and radius vectors of the two MBHs, respectively. This criterion mimics the unresolved condition of the two MBHs being gravitationally bound to each other. The actual coalescence time-

scale is dependent on environmental factors and can vary greatly, but is expected to be around  $10^7 - 10^8$  yr (Armitage & Natarajan 2002; Haiman, Kocsis & Menou 2009; Colpi 2014; Holley-Bockelmann & Khan 2015). These time-scales are small compared to the time-scales of the simulation; while this caveat must be kept in mind, the broader results of merging MBHs still hold.

Black holes can also grow via the accretion of gas. We use a modified Bondi–Hoyle prescription that takes into account the angular momentum of the surrounding gas, and prioritizes the accretion of gas with low angular momentum. If gas is rotationally dominated, the accretion rate is effectively reduced. See Tremmel et al. (2017) for a more detailed description of the model. Our accretion rate  $\dot{M}$  is calculated by the following equation:

$$\dot{M} = \begin{cases} \frac{\pi G^2 \alpha M_{\text{BH}}^2 \rho}{(v_{\text{bulk}}^2 + c_s^2)^{3/2}}, & \text{for } v_{\text{bulk}} > v_\theta \\ \frac{\pi G^2 \alpha M_{\text{BH}}^2 \rho c_s}{(v_\theta^2 + c_s^2)^2}, & \text{for } v_{\text{bulk}} < v_\theta \end{cases}, \quad (1)$$

where  $M_{\text{BH}}$  is the black hole mass,  $\rho$  is the local gas density,  $v_{\text{bulk}}$  is the bulk velocity of the gas,  $v_\theta$  is the tangential velocity of the gas,  $c_s$  is the local sound speed, and  $\alpha = 1$  if the local gas density  $\rho$  is less than the star formation threshold density  $\rho_{\text{th}}$  and  $\alpha = (\rho/\rho_{\text{th}})^2$  if the gas density is greater.

Thermal feedback due to accretion is injected to the nearest 32 particles along the SPH kernel. We disable cooling for the heated particles over the duration of each particle’s own time-step (typically  $10^3 - 10^4$  yr) which mimics the continuous deposition of feedback energy. The feedback energy is proportional to the mass accretion rate  $\dot{M}$ , assuming a radiative efficiency of  $\epsilon_r = 0.1$  and a feedback coupling efficiency of  $\epsilon_f = 0.02$ . All accretion and feedback parameters have been rigorously tested (see Tremmel et al. 2017) and produce galaxies that match observed scaling relations such as  $M_{\text{BH}} - \sigma$ , stellar mass–halo mass, and mass–metallicity. We also point out that the MBHs in the dwarf galaxies we present here undergo very little accretion, due to their wandering nature, so effects due to our choice of subgrid models will be minimal.

A critical component of our black hole model is dynamical friction (DF). This force acts to ‘drag’ black holes, which are far more massive than the sea of stars they exist within, to galaxy centres (and keep them there). Cosmological simulations do not resolve the small scales at which DF acts, because the particle sizes are fairly comparable (within an order of magnitude of each other). We have implemented a subgrid DF model (Tremmel et al. 2015) based on the Chandrasekhar formula (Chandrasekhar 1943; Binney & Tremaine 2008), which estimates the density of stars and dark matter within the unresolved space and adds an additional acceleration, acting as drag on the MBH. This mechanism allows us to accurately trace the dynamics of MBHs in galaxies, which become complicated during mergers and interactions. Black holes which become off-centre experience realistic orbital time-scales, which may or may not be shorter than a Hubble time. We do not include gas particles in the dynamical friction calculation; due to the collisional nature of gas, it may exhibit different dynamical behaviours compared to collisionless particles. The most realistic portrayal of the galactic potential is reflected by the particles not subject to hydrodynamical forces.

Dynamical friction sinking time-scales are dependent on black hole mass, and we acknowledge that the seed masses of MBHs in the early universe are unknown to orders of magnitude. In these simulations, we form black holes via rapid collapse and accretion of gas, which occurs in the most overdense regions. At times, multiple BH particles form at once in the same region, which results

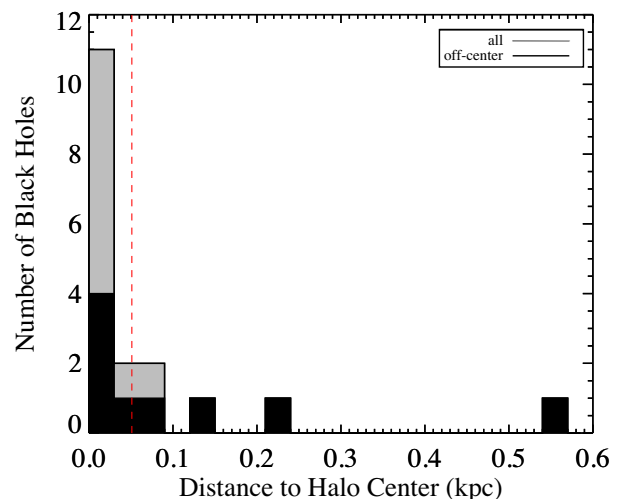


**Figure 1.** Distribution of the physical distance at which MBH seeds form from their halo centres, within 50 Myr of their birth. The grey histogram represents all MBHs that are in dwarfs at  $z = 0$ , and the black histogram line represents those that are off-centre at  $z = 0$ . The vertical red dashed line indicates  $3 \times$  the spatial resolution of the Justice League simulations. Most MBHs form within the resolution limit; however, there are a few that form outside. Overall, the MBHs that are central and off-centre at  $z = 0$  have the same distribution at formation. Only one black hole forms far from its hosts’ centre (Rogue 1).

in their immediate merger. This process creates an approximate initial mass function (see fig. 1 of Bellovary et al. 2019) with initial black hole masses ranging from the simulation seed mass ( $2.5 - 5 \times 10^4 M_\odot$ ) to above  $10^6 M_\odot$ . These values bracket the high end of the range of theorized seed masses. High masses result in more efficient dynamical friction, so an overestimate of seed masses would *overestimate* the number of central MBHs. The fraction of wandering MBHs in dwarfs presented here can thus be seen as a lower limit to the true number, which could be much higher if the black hole seeds were orders of magnitude less massive.

We also note that there are a handful of black holes in our simulations which do not meet the minimum mass criterion for resolved DF, which is  $M_{\text{BH}} > 3M_{\text{dark}}$ . We exclude these objects from all analysis.

### 3 DEPARTURE FROM GALAXY CENTRES

MBHs form in small haloes ( $10^8 M_\odot < M_{\text{halo}} < 10^9 M_\odot$ ; Bellovary et al. 2019) at very early times ( $z < 6$ ). The majority of MBHs form in their galaxy centres. We emphasize that the black holes do not ‘know’ where the galaxy centre is, and are not placed (or fixed) there artificially. They simply form where the gas is densest and collapsing, and meets the criteria for seed formation. In Fig. 1, we show the distribution of distances to galaxy centres shortly after seed formation. Galaxy centres are found using a shrinking-sphere methodology. The time after seed formation varies, because simulation snapshots are saved every  $\sim 50$  Myr, while seed MBHs can form on very small time-steps; the distance shown here is recorded less than  $\sim 50$  Myr after the MBH forms. The MBHs that eventually become off-centre are depicted with a black histogram, while all MBHs in dwarfs are depicted with the grey histogram. The red dashed line represents our spatial resolution. Most MBHs form within this range, though a few form outside. Overall, the distributions are

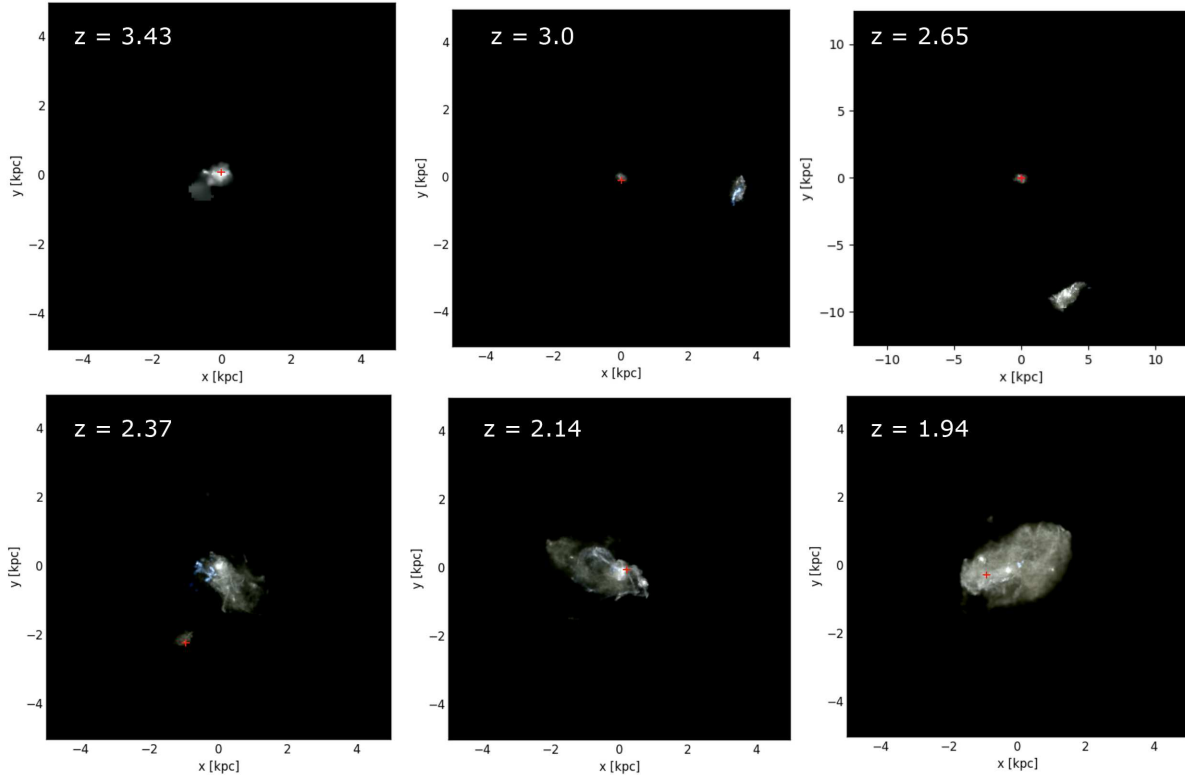


**Figure 2.** Simulated SDSS *rgb* images of a galaxy merger in which a very small galaxy hosting an MBH (designated by a red cross) merges with a larger galaxy, resulting in an off-centre MBH in the larger galaxy. Redshifts are noted in the top left panel of each image.

equivalent the two MBH populations, with the exception of Rogue 1, which is discussed below.

The host galaxies subsequently grow by smooth accretion and/or mergers with other galaxies. As we will demonstrate in this paper, MBHs tend to remain central for galaxies that grow primarily by smooth accretion. Off-centre black holes are likely to be found in galaxies that experience mergers; the most common scenario consists of a minor merger in which the *smaller* galaxy hosts the MBH. As this galaxy collides with a larger galaxy, the MBH’s host is tidally stripped, leaving it to wander in the remnant’s halo. We define off-centre MBHs as existing more than 400 pc from the galaxy centre at  $z = 0$ , which is over twice our force resolution in the lower resolution simulations. An example of this scenario is depicted in Fig. 2, where we show simulated images of a galaxy in the Storm simulation. At  $z = 3.4$ , the tiny dwarf is isolated and hosts a central MBH. In the next two snapshots, one can see a more massive neighbour galaxy approaching. At  $z = 2.14$  the galaxies merge, and by  $z = 1.94$  one can see the merger is complete, with the MBH located towards the left edge of the galaxy. This scenario of the smaller galaxy hosting the MBH is common to all merger-caused off-centre MBHs. There is one case where the larger host *also* hosts an MBH; the galaxy Storm 2 (seen in Fig. 2) accretes another just after 10 Gyr. Since the existing MBH is already wandering, there is no noticeable effect when the additional MBH is added.

We show a graphical representation of this galaxy merger in the storm simulation in Fig. 3. We define ‘merger’ as the moment when a satellite galaxy can no longer be distinguished by the halo finder [as opposed to the moment the satellite enters the virial radius ( $R_{\text{vir}}$ ) of the host, which happens earlier]. In this three-panel plot, the top panel shows the distance of the MBH from the centre of its host galaxy. The

MBH in Fig. 3 is the first to merge with the larger host, which occurs at the moment the distance suddenly jumps to a larger value (shown by a red dashed line in all panels). This jump occurs because the satellite host of the MBH has been disrupted, and the new host is the larger galaxy. The centre panel shows the stellar mass of the MBH’s host galaxy as a function of time. At the moment of the merger, the stellar mass also makes a sudden jump, which reflects the fact that the MBH has suddenly entered a much larger host galaxy. The bottom panel shows the bolometric accretion luminosity of the MBH versus time, in bins of 10 Myr. After an initial burst, the luminosity remains around  $\sim 10^{38}$  erg s $^{-1}$  for several Gyr. As the MBH moves further away from the galaxy centre, however, the mean luminosity also decreases. For more discussion regarding luminosity, refer to Section 5.1.

We show the wandering nature of all BHs together in Fig. 4, where we plot the distance from the galaxy centre versus time for each object. There are no cases where a BH is dislodged from the centre and eventually returns there for the long term, nor are there cases where a central MBH experiences a merger and remains central. In fact, mergers at late times can cause MBHs to move *even further* from their hosts’ centres. In this figure, each MBH is depicted in a different colour and panel. We place a coloured circle at the end of each line for clarity. Larger stars at times between 0 and 13.8 Gyr represent galaxy mergers, which act to perturb the MBH from the centre. The galaxy Storm 2 experiences two such mergers (at 3 and 10 Gyr, the latter displacing the pink MBH a second time). The galaxy Sandra 6 has a merger at 9 Gyr, but we note the MBH is already off-centre at this time. We suspect there was an earlier merger before 4 Gyr, but the time resolution of our simulation outputs for Sandra is poor, and we cannot confirm when this putative merger may have taken place.



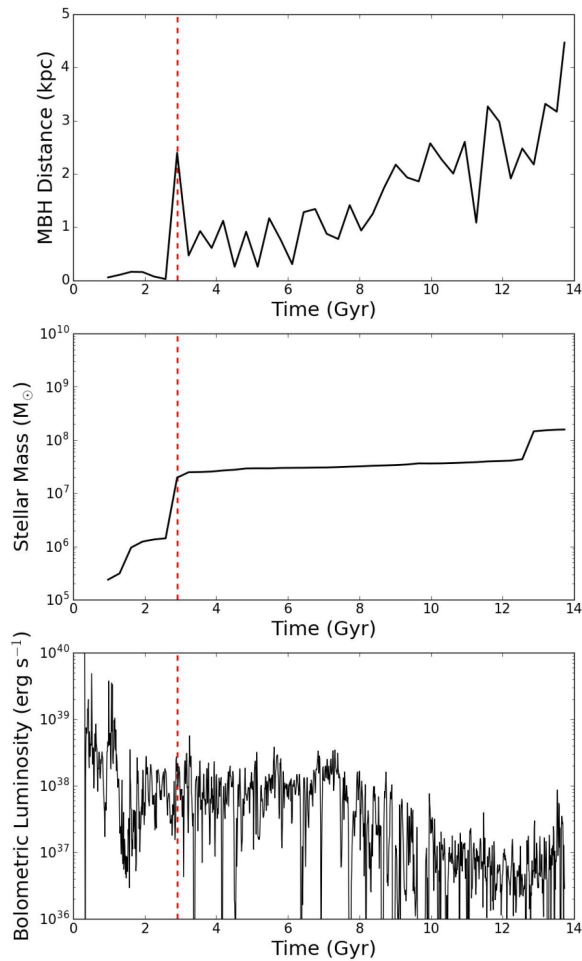


**Figure 3.** *Top panel:* Distance of an MBH to the centre of its host halo versus time. It enters a much larger halo at  $\sim 2.5$  Gyr, resulting in a sudden increase in distance to the centre of its (new) host. *Middle panel:* Stellar mass of the MBH’s host galaxy versus time. The time of the galaxy merger is easily seen when the host mass rises suddenly. *Bottom panel:* Bolometric accretion luminosity versus time of the MBH, binned in 10 Myr intervals. The luminosity decreases as the MBH departs the central regions, due to lower gas densities. In all panels, the red dashed line indicates the time the MBH leaves the centre of its host halo.

These three MBHs are examples of distances *increasing* with time, as compared to the other five that remain approximately constant (while oscillating). Our results are consistent with observations by Reines et al. (2020), in which the off-centre compact radio sources are located between 1 and 5 kpc from the optical centres of their host galaxies.

Mergers with other galaxies are the cause of the displacement of MBHs in all but one case (Rogue 1, though possibly also Sandra 6). In Table 1, we show the properties of off-centre MBHs and their host galaxies. The column  $z_{\text{off}}$  represents the redshift at which the MBH becomes off-centre when perturbed by a merger. In all of these cases, the MBH is hosted by the ‘minor’ galaxy in the merger, and coalesces with a more massive galaxy. The resulting tidal stripping of the smaller galaxy leaves its remains orbiting in the halo of the primary galaxy. The larger galaxy often lacks an MBH itself, which is a consequence of our MBH seed formation model. To mimic the ‘direct collapse’ scenario, we require gas to have a low  $\text{H}_2$  fraction to form MBHs, while stars form with a high  $\text{H}_2$  fraction. As a result, gas in galaxies which form first (and are often larger as a result) will

meet the criteria for star formation, but not MBH formation. MBHs form from gas that has likely been heated by nearby star formation, consistent with the direct collapse model (Spaans & Silk 2006).

Overall, off-centre MBHs are less massive and located in more massive hosts than those with central MBHs. In Fig. 5, we plot MBH mass versus host galaxy stellar mass (which is multiplied by 0.6 to correct for observational bias; Munshi et al. 2013). Points are coloured by the log of the distance to the halo centre, with light circles representing central MBHs and darker green points representing further offset MBHs. Dark green points are primarily located in the quadrant containing larger host stellar masses and lower MBH masses. These instances occur when tiny MBH-hosting galaxies merge with larger (and often) MBH-less galaxies. The larger hosts swallow the remains of the small galaxies, but the bulk of the disruption occurs in the outskirts of the larger galaxy. These larger galaxies are still dwarfs; they do not have deep enough potential wells for dynamical friction to act to bring the MBH to the centre. The lower MBH masses also result in longer dynamical friction time-scales, slowing their journey to the centre as well (see Section 4).

The outlier in this story is the MBH in the largest galaxy of the Rogue simulation (known as Rogue 1). The black hole forms around  $z = 11$ , but our first simulation snapshot is recorded 540 Myr later. At that moment, the host galaxy is extremely bursty and messy, consisting of many clumps of localized star formation. Due to our lack of time resolution at very high redshift, we cannot determine whether the MBH forms centrally and is quickly perturbed, or whether the MBH forms in an off-centre clump. Rogue 1 has a very bursty history overall and grows to become the largest dwarf galaxy in our sample (in Fig. 6 it is represented by the topmost density profile). This galaxy is an instance where extremely bursty star formation results in likely off-centre MBH formation, and dynamical friction is not effective enough to bring it to the centre.

#### 4 REMAINING OFF-CENTRE

When MBHs in dwarf galaxies are perturbed from their centres, dynamical friction may be able to bring them back over time. In massive and/or smooth galaxies, this process is expected to be efficient, due to the dense stellar populations (e.g. galaxy bulges) surrounding SMBHs. Dwarf galaxies have a variety of morphologies, but in general they have a lower central stellar density than their massive counterparts, a clumpier structure, and a smaller scale radius as well. Thus, when an MBH leaves the centre, it is more likely to travel to a region of low density (possibly outside of the main stellar component of the galaxy) and has a much more tenuous stellar background to move through on its way back to the centre. As a result, dynamical friction time-scales are quite long for these MBHs, which may take tens of billions of years to return to their galaxies’ centres. This phenomenon of non-sinking seeds is also explored in detail in Ma et al. (2021), who also find that dynamical friction time-scales are longer than a Hubble time when MBHs are perturbed from the centres of clumpy, high-redshift galaxies.

To calculate dynamical friction time-scales, we employ the following equation from Binney & Tremaine (2008):

$$t_{\text{df}} \sim \left( \frac{19 \text{ Gyr}}{\ln \Lambda} \right) \left( \frac{r_i}{5 \text{ kpc}} \right) \left( \frac{\sigma}{200 \text{ km s}^{-1}} \right) \left( \frac{10^8 M_{\odot}}{M_{\text{BH}}} \right), \quad (2)$$

$\Lambda$  is assumed to be equal to  $b_{\text{min}}/b_{\text{max}}$ , where  $b_{\text{max}}$  is the maximum impact parameter (which we set equal to the  $z = 0$  radius of the MBH orbit,  $r_i$ ), and  $b_{\text{min}}$  is the minimum impact parameter (set to 10 pc to represent the characteristic size of nuclear star clusters, which commonly exist around lower mass SMBHs). We directly measure

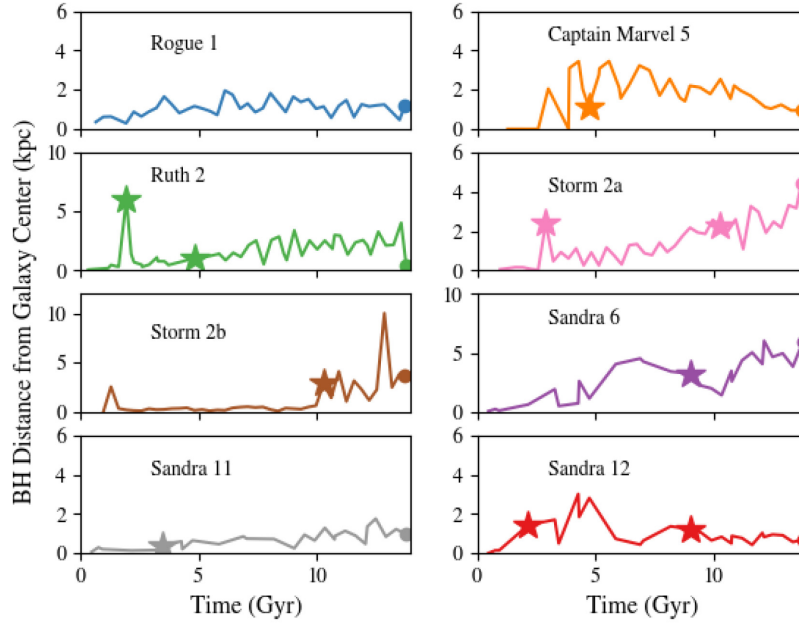


**Figure 4.** Each panel represents a different wandering MBH, as shown by the labels. Larger stars during MBH evolution represent galaxy mergers, which act to perturb the MBH from the centre. Circles at 13.8 Gyr mark the final position for clarity.

**Table 1.** Off-centre MBH and galaxy properties, including Halo ID at  $z = 0$ , black hole mass  $M_{\text{BH}}$ , the redshift of offset  $z_{\text{off}}$ , stellar mass  $M_*$ , distance to the galaxy centre  $r_i$ , stellar velocity dispersion  $\sigma$  measured within  $r_i$ , and dynamical friction time-scale  $t_{\text{df}}$ . Stellar masses are multiplied by an observational correction factor of 0.6 as described in Munshi et al. (2013).

Simulation name	Halo ID	$M_{\text{BH}}$ ( $M_\odot$ )	$z_{\text{off}}$	$M_*$ ( $M_\odot$ )	$r_i$ (kpc)	$\sigma$ ( $\text{km s}^{-1}$ )	$t_{\text{df}}$ (Gyr)
Sandra	6	$3.1 \times 10^5$	3.0	$1.99 \times 10^8$	6.9	10.8	69.1
Sandra	11	$3.3 \times 10^5$	1.9	$8.12 \times 10^7$	1.0	8.9	11.4
Sandra	12	$1.2 \times 10^6$	3.0	$6.26 \times 10^7$	0.78	32.7	9.4
Ruth	2	$2.5 \times 10^5$	3.3	$4.50 \times 10^8$	0.46	13.0	12.1
Captain Marvel	5	$2.4 \times 10^5$	1.6	$7.33 \times 10^6$	1.0	3.3	5.6
Rogue	1	$2.5 \times 10^5$	8.1	$9.86 \times 10^8$	2.4	47.1	158
Storm	2	$2.0 \times 10^5$	2.4	$9.48 \times 10^7$	4.9	18.5	140
Storm	2	$7.6 \times 10^4$	0.3	$9.48 \times 10^7$	3.8	18.5	297

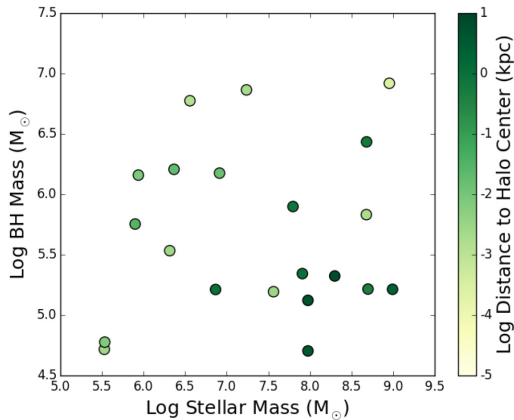


**Figure 5.** Log MBH mass versus Log of the stellar mass for all dwarf galaxies hosting MBHs at  $z = 0$ . Points are coloured by the log of the distance of the MBH to the galaxy centre, with darker green points being more off-centre. Off-centre MBHs are typically of lower mass but hosted in dwarfs with larger stellar masses.

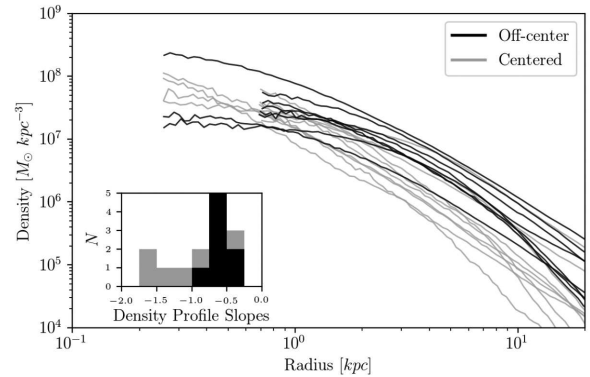


**Figure 6.** Density profiles of all MBH-hosting dwarf galaxies in our sample. Dark lines represent galaxies with off-centre MBHs, and grey lines represent those with central MBHs. The inset shows a histogram of the slopes of the inner density profiles, with the black histogram representing galaxies hosting off-centre MBHs. All of the galaxies with off-centre MBHs exhibit cored profiles.

$\sigma$ , the velocity dispersion, of all of the star particles within  $r_i$  in each galaxy. To ensure we are making a conservative estimate of the DF time-scales, we add a factor of 50 per cent to the mass of each MBH, to account for the additional mass of a possible nuclear star cluster, which will shorten the DF time-scale estimate. These time-scales are not affected by the low densities in galaxy outskirts, because the subgrid model interpolates the unresolved density. Even for a higher resolution simulation with more star particles, the unresolved density would not be affected as long as the background density of stellar (and dark matter) mass is the same. The dynamical friction model has been tested at a range of resolutions and is found to match the Chandrasekhar estimate well at the resolutions we use here, even in cases of low particle density.

In Table 1, we present information for each off-centre MBH. We acknowledge that as the distance of each MBH to its galaxy centre changes, the values of  $t_{\text{df}}$  will vary, and thus using  $r_i$  at the present time ( $z = 0$ ) gives a basic estimate of this time-scale. Even as an order-of-magnitude estimate, however, one can see that the majority of the time-scales are longer than a Hubble time, which does not change when using a different radius. For the majority of these off-centre MBHs, they will effectively never return to the centres of their hosts.

The shape of the potential well in dwarf galaxies is another reason why their MBHs may remain off-centre; defining a ‘centre’ is not always trivial. For example, the Large Magellanic Cloud has been reported to have several conflicting measured centres (e.g. HI kinematics, stellar kinematics, and photometry each give a different answer; van der Marel & Kallivayalil 2014). Dwarf galaxies are often irregularly shaped, and also often exhibit cored density profiles (Moore 1994; Relatores et al. 2019). This is the case in our simulated galaxies as well, as shown in Fig. 6. Dark lines represent galaxies which host off-centre MBHs, and grey lines represent those with central MBHs. The distribution of inner slopes is shown in the inset, with the grey depicting all galaxies and the black region galaxies hosting off-centre MBHs. We fit the dark matter profiles using the core-Einasto profile presented in Lazar et al. (2020). To derive the inner slope, we fit from a line to the profile from our innermost resolved radius (set conservatively to four times the gravitational softening) out to 1–2 per cent of the  $R_{\text{vir}}$ . We use the slope of this line ( $\alpha$ ) as the core slope we present in Fig. 6. Slopes steeper than  $-1$  are considered to be cuspy, whereas slopes that are less than  $-1$  to 0 are showing core formation, or large cores.

All galaxies hosting off-centre MBHs have central densities with flat slopes, indicating cored profiles; galaxies with central MBHs have a combination of cored and cuspy profiles. Past simulation work has demonstrated that cored profiles in dwarfs have been shown to be a result of a redistribution of mass by driven by supernova feedback (e.g. Governato et al. 2012). Dwarfs with cuspy profiles likely have less bursty star formation histories. Due to the shallow shapes of cored profiles, a displaced MBH does not feel a strong gravitational pull to the galaxy centre. Instead, it may experience core-stalling, ‘sloshing’ around within the inner region (typically 1–2 kpc) without settling into one location. 50 per cent of the off-centre MBHs in our sample are located within the approximate ‘core’ region of their galaxies, and all of those have existed within a mean radius of 2 kpc or less for the majority of their off-centre lifetimes, indicating approximate core-stalling behaviour. (The dynamical friction subgrid model prevents a literal ‘stall’ because it continually acts, but the time-scales are still very long, effectively stalling the orbital decay.) In fact, only those galaxies that experience recent mergers have MBHs that are outside of the central core (see Section 3).

One might ponder how these results might change with a different seed model, e.g. ‘light’ seeds (from Population III stars) plus efficient early growth. With such a model, seed formation is much more efficient, and we might expect every dwarf galaxy to host (at least one) MBH. The masses of such seeds are poorly constrained, but we can conjecture that they may be around  $\sim 1000 M_{\odot}$ . These seeds are not constrained to form in galaxy centres, and so their initial locations within galaxies would vary. Due to their lighter masses, they would experience even weaker dynamical friction forces compared to their ‘heavy’ counterparts. Thus, one might expect an even greater number of wandering MBHs in dwarf galaxies, whether or not they have undergone galaxy mergers, since the efficiency of orbital decay to the central region decreases. On the other hand, with a greater number comes a greater statistical likelihood of an MBH undergoing something more interesting, like settling into the centre, or increasing its mass rapidly (perhaps by undergoing a large accretion event or merging with another MBH). Overall, we postulate that light seeds would result in an increased number of (lower mass) wandering MBHs, but a buildup of a more massive central MBH cannot be ruled out. Cosmological simulations with such small particles run to  $z = 0$  are extremely computationally intensive, but this topic would be worthwhile to pursue in future work.

## 5 DETECTING OFF-CENTRE MBHS

Our work shows that off-centre MBHs in dwarfs maybe be fairly common, especially for those with larger stellar masses, due to the combination of a higher MBH occupation fraction (Bellovary et al. 2019) and higher off-centre incidence with increasing  $M_*$ . Recently, observations have uncovered evidence for these objects as well. In Reines et al. (2020), they examined radio-selected dwarf galaxies and found 13 with clear signatures of compact radio sources due to AGN, and approximately half of these are off-centre. Subsequently, Mezcua & Domínguez Sánchez (2020) used spatially resolved emission-line diagnostics to detect AGN signatures in 37 dwarf galaxies. They report that in most cases the AGN emission is offset from the photometric centre of the galaxy, possibly indicating off-centre MBHs. In this section, we address the detectability of our simulated off-centre MBHs, both electromagnetically and via dynamical signatures.

### 5.1 Luminosity

We calculate a bolometric luminosity due to accretion on to the MBH using the formula  $L = \epsilon_f \epsilon_r \dot{M} c^2$ , where the accretion rate  $\dot{M}$  is described by equation (1) and is dependent on the density of the surrounding gas. Gas in galaxy haloes tends to be quite diffuse, resulting in relatively low MBH accretion rates compared to galaxy centres. The accretion rate also depends on the relative velocity between the MBH and the surrounding gas ( $v_{\text{bulk}}$ ), which is much larger for an MBH drifting through its host galaxy compared to one residing stationary at the centre. It is also worth noting that the MBHs in dwarfs have categorically lower masses compared to SMBHs in galaxy centres. As a result of the lower densities, higher velocities, and lower black hole masses, substantial accretion rates are not expected.

Fig. 7 shows light curves for every off-centre MBH in a dwarf from the time of formation to  $z = 0$  (excepting the Storm 2A MBH light curve that is shown in Fig. 3). The luminosities are binned in 10 Myr intervals. We point out that the y-axis shows bolometric luminosity, so the luminosity in any given part of the electromagnetic spectrum (e.g. X-rays) will be at least 10 per cent of this value. Each curve

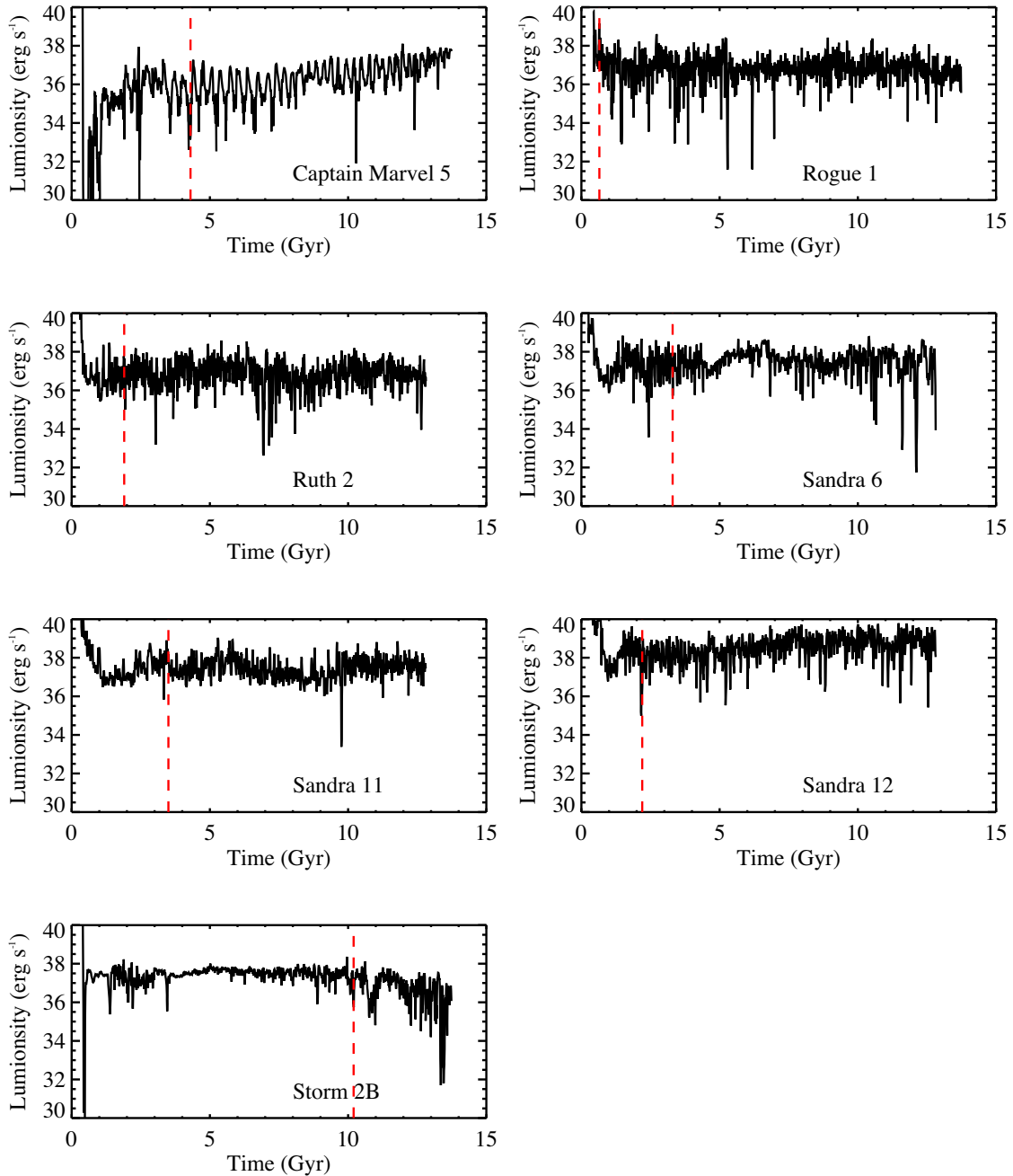


**Figure 7.** Bolometric luminosity versus time for every MBH that resides off-centre in a dwarf galaxy at  $z = 0$ . Luminosities are binned in 10 Myr intervals. The simulation name and halo ID are labelled on each plot. All MBHs are below detectability thresholds at all times, and luminosities either are unchanged or decrease once they become off-centre. The red dashed vertical lines indicate the moment the MBHs become off-centre.

is highest just after the MBH forms, which is an artefact of MBH formation in ChaNGa. Because seeds form from cold dense gas, they undergo a short accretion event before their accretion feedback can heat the gas. Once feedback occurs, the surrounding gas quickly reaches an equilibrium in density and temperature.

All of the light curves vary dramatically, but maintain average values around  $10^{36}$ – $10^{38}$   $\text{erg s}^{-1}$ . At the moment they become off-centre (shown by the dashed red line), some of the mean luminosities tend to decrease, due to the decrease in ambient gas densities and increase in  $v_{\text{bulk}}$ . Other MBHs undergo little luminosity change at all. Accounting for bolometric corrections, none of these simulated off-

centre MBHs can be easily distinguished as such by electromagnetic radiation at any point in their histories.

While this result is an apparent contradiction to observations by Reines et al. (2020) and Mezcua & Domínguez Sánchez (2020), we point out that our sample size is quite small. These and other works report AGN fractions in dwarfs of a few per cent or less (Reines et al. 2013; Pardo et al. 2016; Mezcua et al. 2018), suggesting that the conditions for MBHs to exist as AGN in dwarfs are quite rare. We also point out that our calculated luminosities depend on a modified Bondi–Hoyle accretion model, which may not be an accurate representation of the physical situation. Additionally,



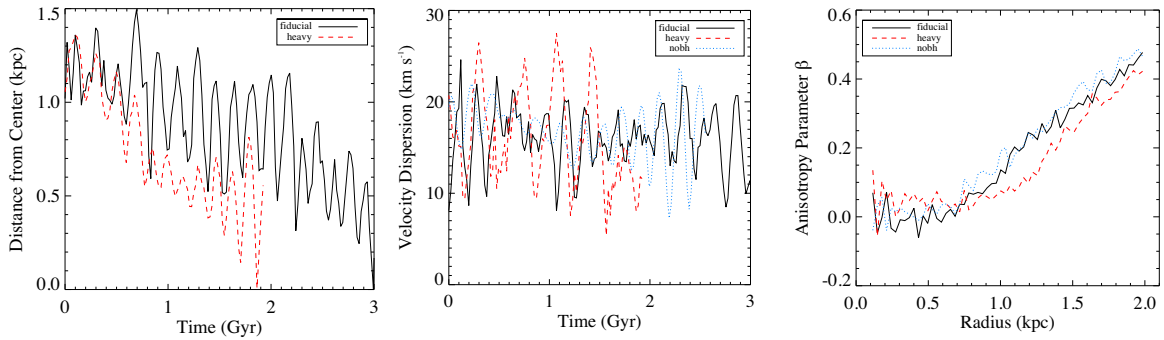


**Figure 8.** *Left:* The distance of the MBH from the galaxy centre versus time. *Centre:* The velocity dispersion of the stars in the galaxy versus time. *Right:* Anisotropy profiles of each galaxy after 2 Gyr of evolution. In all figures, the black solid line represents the fiducial run, red dashed line is the heavy BH run, and the blue dotted line is the run with no MBH.

several of our MBH host galaxies have stellar masses less than  $M_* < 10^8 M_\odot$ , and there are very few reliable detections of AGN in such small galaxies. If we add the complications of wandering to this situation, it is not surprising that off-centre MBHs with high accretion rates in dwarfs are extremely rare. Rather, it is perhaps surprising that off-centre MBHs have been detected electromagnetically in dwarfs at all.

The existence of a nuclear star cluster could improve the situation, however. Lower mass SMBHs tend to have nuclear star clusters (Böker 2010), which may remain bound to a perturbed MBH. The luminosity of the stars in the cluster would increase the likelihood of detecting an off-nuclear point source. Additionally, if one of the bound stars becomes dynamically perturbed, it may interact with the MBH and create a tidal disruption event or similar hyperluminous X-ray source. The object HLX-1 (Farrell et al. 2009) is an example of such a candidate, and is consistent with a dwarf galaxy that hosts an MBH disrupting an orbiting star (Lasota et al. 2011). While we cannot resolve nuclear star clusters or tidal disruption events, it is worth keeping these scenarios in mind when discussing observability.

## 5.2 Dynamics

While MBHs are not observable due to their accretion luminosity, their effects may be discernible dynamically, via their interactions with stars. A massive object may ‘stir’ stars in the galaxy, creating an increased velocity dispersion, altered anisotropy profile, or other noticeable signature. Such an effect is not measurable in our cosmological simulations, which do not resolve the radius of influence of the MBH. We have thus followed up on this concept by further ‘zooming’ in and resimulating dwarfs with off-centre MBHs at higher resolution.

The galaxy we selected for further study is the fifth most massive galaxy in the Captain Marvel simulation (hereafter the fiducial simulation); it has a stellar mass of  $1.2 \times 10^7 M_\odot$  and a total halo mass of  $8.6 \times 10^9 M_\odot$ . The MBH is 1.0 kpc from the centre at  $z = 0$  and has a mass of  $1.6 \times 10^5 M_\odot$ . This halo has a benign history since its last major merger at  $z \sim 1.4$ , which initially caused the off-centre MBH, and exists in isolation. We made a spherical cut-out of the  $z = 0$  galaxy at the virial radius, and increased the particle number by a factor of 8. The resulting galaxy has over 11 million total particles, with masses  $M_{\text{gas}} = 70 M_\odot$ ,  $M_{\text{star}} = 32 M_\odot$ , and  $M_{\text{dark}} = 832 M_\odot$ . Star and dark matter particles were split by placing new particles along a 3D Gaussian kernel centred on the parent particle, while for gas particles we replaced the particle with eight particles at the corners

of a cube of size 0.5 the mean interparticle separation, and then rotated that cube to a random orientation. The MBH particle was not split. The gravitational softening values of particles were decreased substantially to 0.5 pc, in order to resolve the sphere of influence of the MBH. We ran this simulated galaxy in isolation for two billion years, as well as two additional simulations; an identical one without an MBH (hereafter known as ‘nobh’), and an identical one but with the MBH mass increased by a factor of 10 (referred to as ‘heavy’). Comparing these three simulations allows us to determine whether the effect of the MBH is noticeable compared to a galaxy without one, as well as to the case where the galaxy hosts an unreasonably large MBH (10 per cent the mass of the entire stellar population).

Our goal with this experiment is to resolve the effects of both dynamical friction and two-body relaxation directly. The black hole is far more massive than the surrounding particles, and thus will exchange energy with stars during gravitational interactions on small scales. As a result, the MBH will lose energy and sink to the centre of the potential well, while star particles will gain energy as their velocities are increased. We aim to determine if this increase in stellar velocity is measurable, compared to a galaxy which does not host a wandering MBH.

In the left-hand panel of Fig. 8, we show the distance of the MBH from the galaxy centre versus time. The heavier MBH, represented by the red dashed line, experiences stronger dynamical friction forces and sinks to the centre more quickly, but does not quite get there within 2 Gyr. The lighter MBH, shown with the black solid line, does experience dynamical friction but not enough for it to settle into the centre within the following 3 Gyr. These time-scales are consistent with the Chandrasekhar dynamical friction estimate mentioned in Table 1, i.e. we calculated  $t_{\text{df}} = 5.6$  Gyr for the fiducial case studied in this section.

One might expect an increased velocity dispersion in a galaxy with an MBH (and a larger increase with a larger MBH), because gravitational interactions between the MBH and close-passing stars will cause stars to accelerate, thus increasing the velocity dispersion. The dynamical situation is complicated, however, by the ‘breathing’ nature of this galaxy, where episodic star formation causes semiperiodic expansion and contraction of the galaxy (see Stinson et al. 2007). Comparing the velocity dispersion of the stars over time, the central panel of Fig. 8 shows that while the total dispersion varies over time in an oscillatory way, the minimum and maximum values are approximately equal, and no discernible difference exists. Even in the case of the heavy MBH, the extrema of the values of the velocity dispersion are a bit larger than in the other cases, but not different enough for an observer to measure an anomalous dynamical state.

We suspect that the lack of difference is because there are few stars within the MBH's radius of influence at any given time.

Calculating the radius of influence ( $R_{\text{infl}} = GM_{\text{BH}}/\sigma^2$ ) for each MBH, we find 2.7 pc for the fiducial case and 38 pc for the heavy case. (Note that the force softening is 0.5 pc in both cases.) These estimates of  $R_{\text{infl}}$  are when the MBH is in the denser regions of the galaxy; however, each MBH spends substantial time at the galaxy outskirts, when there are few or no star particles within  $R_{\text{infl}}$ . The median number of star particles within  $R_{\text{infl}}$  varies with the MBH's position, but in denser regions comes to  $\sim 1$ –2 for the fiducial case and  $\sim 40$  for the heavy case. We also emphasize that being within  $R_{\text{infl}}$  is not identical to being bound, because both the MBH and stars are moving on their own trajectories. The stars within  $R_{\text{infl}}$  at one moment are different from those within  $R_{\text{infl}}$  the next. We propose a modified calculation for  $R_{\text{infl}}$  for a moving MBH:  $R_{\text{infl, moving}} = GM_{\text{BH}}/(\sigma^2 + v_{\text{BH}}^2)$ , which takes into account the movement of the MBH and effectively reduces the radius of influence. Using this modified value, we recalculate  $R_{\text{infl, moving}} = 1.3$  pc for the fiducial case and 15 pc for the heavy case, with median value of 0 and 15 enclosed particles within each, respectively. These lower numbers indicate that a moving MBH has a much lower chance of gravitationally influencing nearby stars. Overall, this dwarf galaxy has a much lower stellar density than e.g. a galaxy bulge or nuclear star cluster, and so the MBH's gravitational influence is negligible on the stellar dynamics. We have also investigated the potential effect of the MBH on the dynamics and structure of each galaxy's dark matter and gas properties, and find no measurable differences.

Velocity anisotropy is a dynamical tool which has been used to infer the presence of (albeit central and unmoving) SMBHs (e.g. Binney & Mamon 1982; van der Marel 1994). This quantity is a function of the velocity dispersion in the tangential direction  $\sigma_\theta$  and the velocity dispersion in the radial direction  $\sigma_r$ , and is defined as

$$\beta = 1 - \sigma_\theta^2 / 2\sigma_r^2. \quad (3)$$

When measured in spheroidal galaxies, the velocity anisotropy typically ranges from  $\beta = 0$  at galaxy centres (where stellar orbits are predominantly isotropic) to  $\beta = 1$  at galaxy outskirts (where radial orbits dominate). We measure the anisotropy profiles of our three models after 2 Gyr of independent evolution (right-hand panel of Fig. 8). The anisotropy profiles of the stellar populations are effectively identical in all three cases, which is not surprising since the MBH is not stationary, and the stars do not have time to adjust their orbits to its gravitational potential.

The star formation histories of the three cases are also extremely similar. In Fig. 9, we show the star formation rate versus time for the three simulations, which begin nearly identically and then diverge. However, the rates do not deviate from each other significantly. One might expect additional quenching due to the presence of the MBH, but its movement prevents the accretion of substantial gas and thus any feedback effects. One might also expect the passage of the MBH to trigger bursts of star formation by perturbing gas clouds, but this effect is not seen either.

The accretion luminosity of the MBH is not high enough to be detectable at any point. In Fig. 10, we show the bolometric accretion luminosity versus time for both simulations with MBHs. Due to the wandering nature of the black holes and the diffuse gas in the galaxy, there is little opportunity to accrete a substantial amount of gas at any given time. The heavier MBH has a larger luminosity, which is expected due to the nature of our accretion model ( $\dot{M} \sim M_{\text{BH}}^2$ ). However, since both MBHs have a high relative velocity with respect to the gas, the accretion rate remains low. Assuming a simple bolometric correction factor of 10 per cent for X-rays in the 2–10 keV

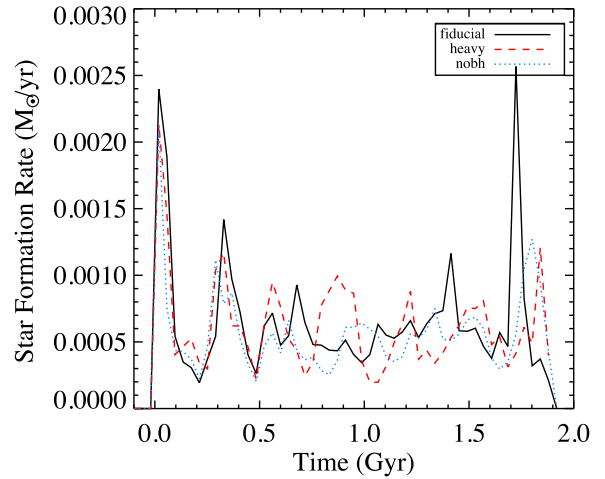


**Figure 9.** Star formation history for the fiducial, heavy, and no MBH runs. Lines are as in Fig. 8.

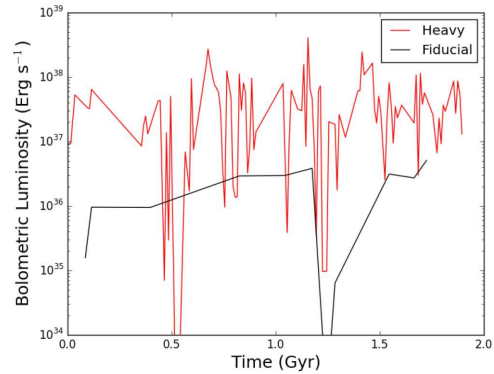


**Figure 10.** Bolometric luminosities for the wandering MBHs in the isolated simulations, averaged over intervals of 10 Myr. The black line is the fiducial simulation, while the red line is the heavy black hole.

range, an object with  $L_X = 10^{37}$  erg s $^{-1}$  would not be discernible from an X-ray binary system, especially at an off-centre location in the galaxy.

In a more physically realistic accretion scenario, the gas must either become gravitationally bound to or experience a rapid inflow towards the MBH in order to be accreted, which would still be difficult in a case where the MBH is moving quickly through a diffuse medium. Such a scenario is only likely in a galaxy with a larger number of clumps of dense gas (as seen in Reines et al. 2020), which would need to become bound to the MBH as it passes nearby. In Fig. 11, we show gas surface density images of the fiducial isolated galaxy, at  $t = 0$  (effectively at  $z = 0$ ) and at  $t = 3$  Gyr (3 Gyr later). At  $t = 0$ , the MBH is moving through a region of lower gas density. As a result, there is only low-level accretion from passing through this smooth gas. At  $t = 3$  Gyr, the MBH arrives at the galaxy centre. However, the gas distribution is irregular, and there are no clumps that could bind to the MBH. Our simulations are capable of resolving a clumpy interstellar medium, so the lack thereof is not a resolution issue. Without a clumpy medium, an overdensity, or a rapid inflow of gas, the MBH accretion will remain fairly quiescent.

We calculate the  $B - V$  colours of each galaxy using the pynbody analysis suite, which uses simple stellar populations models (Marigo et al. 2008; Girardi et al. 2010) to convert stellar ages and metallicities

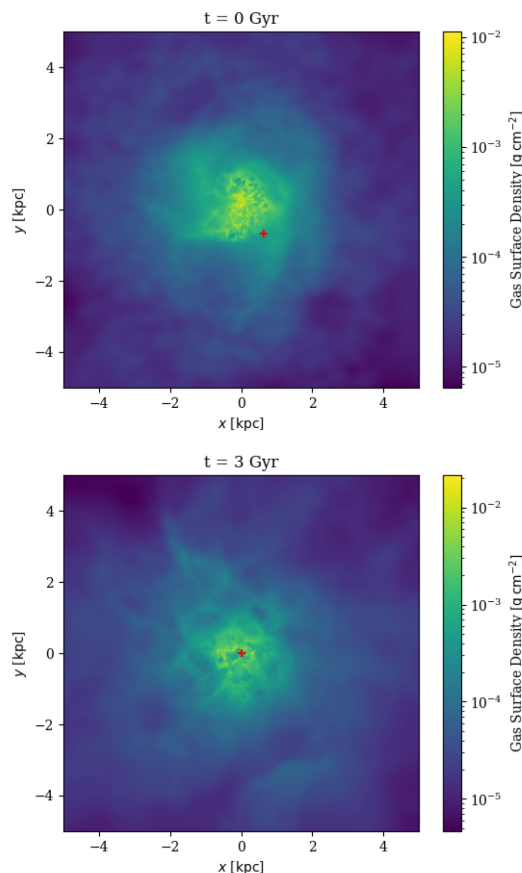


**Figure 11.** Images of projected (two-dimensional) gas density for the fiducial galaxy at  $t = 0$  Gyr (top) and  $t = 3$  Gyr (bottom). The MBH is marked with a red cross. The colour bar indicates gas density. The MBHs do not experience substantial accretion events because the surrounding gas is diffuse.

to luminosities and subsequently magnitudes. Including all stars in the galaxy in our analysis, the resulting colours are  $(B - V)_{\text{noBH}} = 0.507$ ,  $(B - V)_{\text{fiducial}} = 0.527$ , and  $(B - V)_{\text{heavy}} = 0.535$ . While the MBH-hosting galaxies are technically redder than their MBH-less counterpart, the difference is minuscule, and not detectable.

## 6 SUMMARY

Consistent with recent observations (Reines et al. 2020), zoom-in cosmological hydrodynamical simulations show that about 50 per cent of MBHs in dwarf galaxies are not located in the centres of their hosts. In this paper, we examine the dynamical histories of these MBHs and analyse the likelihood of detecting them.

MBHs form in very low mass haloes ( $10^8 - 10^9 M_\odot$ ) and nearly always form centrally. These MBH host galaxies undergo mergers with more massive dwarfs (often *not* hosting an MBH) during their evolution. This merger perturbs the matter in both galaxies, but often results in the MBH host being tidally disrupted by the larger galaxy. The remains of the original MBH host thus join the components of the larger dwarf’s stellar halo, where the MBHs are seen wandering. However, in one case out of eight, the black hole does form off-centre and remains so; thus, it is possible that a small fraction ( $\sim 10$  per cent) of off-centre MBHs are not due to perturbations from mergers. Indeed, factors other than those described here may also contribute to wandering MBHs in dwarfs, such as perturbations from merging

subhaloes (Boldrini, Mohayaee & Silk 2020) or gravitational recoil (e.g. Blecha et al. 2011).

The combination of dwarfs exhibiting cored density profiles and low stellar densities results in long dynamical friction time-scales. As a result, the MBHs that enter galaxies via mergers do not sink to the centre within a Hubble time. The most likely off-centre MBH hosts are galaxies with larger stellar masses (i.e. more likely to have acquired a smaller galaxy in a merger) and smaller MBH masses (resulting in weaker dynamical friction forces).

These off-centre MBHs are extremely difficult to detect. Their accretion rates are very low due to the low density of gas in galaxy haloes and the high relative velocities of the MBHs themselves. The accretion luminosities of these objects are low enough to be either undetectable or easily confused with another object, such as an X-ray binary or background quasar. We also examined whether an off-centre MBH could be detected indirectly via dynamical studies of the surrounding stars. A massive compact object might dynamically heat the stellar system, resulting in larger velocity signatures. Unfortunately, due to the low masses of the MBHs and the low stellar densities, there are too few stars within the radius of influence of the MBH at any given time to cause any difference in dynamical signatures.

One detection method we do not explore in this work is strong gravitational lensing. Banik et al. (2019) predict that wandering IMBHs can distort the lensing arcs formed by dark matter haloes when they cross the line of sight either in the foreground or in the background of the lens. Such distortions can be detected by high-resolution interferometers such as the SKA. Alternatively, Paynter, Webster & Thrane (2021) report a gamma-ray burst that may be lensed by an IMBH, based on a delay in the arrival pulse. We encourage further investigation of this fascinating detection method, which is beyond the scope of this paper.

While the lack of detectability of off-centre MBHs is disappointing for those who seek to find more of them, we remind the reader that our sample size is very small. The AGN fraction of dwarf galaxies is already quite low ( $< 1$  per cent; Reines et al. 2013; Pardo et al. 2016; Mezcua et al. 2018), and this estimate is for central MBHs. Simply based on statistics, one does not expect to find a luminous AGN in a sample as small as ours. For a larger sample, in future work we will look to the ROMULUS simulation (Tremmel et al. 2017), which hosts 492 dwarf galaxies (defined as isolated and with stellar masses  $10^8 M_\odot < M_* < 10^{10} M_\odot$ ); 228 of these host MBHs (Sharma et al. 2020). Repeating our analysis on this larger sample will provide new insights into the causes and detectability of off-centre MBHs.

## ACKNOWLEDGEMENTS

The authors thank the anonymous referee, who asked helpful and interesting questions. JMB is grateful for the support of the AstroCom NYC project (National Science Foundation (NSF) AST-1153335). JMB and SH acknowledge support from NSF AST-1812642. SH is grateful for support from the Jack Kent Cooke Foundation. SH, KC, and DR are grateful to NSF Research Experiences for Undergraduates (REU) grant 1359310 and the Queensborough Community College physics department. JMB and ML acknowledge support from the City University of New York (CUNY) Community College Research Grant. AB acknowledges support from NSF AST-1813871. CRC acknowledges support from NSF CAREER grant AST-1848107. FDM and JPS acknowledge support from NSF grant PHY-2013909. FDM, JPS, and JVN acknowledge support from the University of Oklahoma. MT was supported by an NSF Astronomy and Astrophysics Postdoctoral Fellowship under award AST-2001810. JMB thanks



Ray Sharma, Nathan Leigh, Amy Reines, Vivienne Baldassare, Jenny Greene, and Mar Mezcuca for helpful comments, and Avi Loeb for suggesting the dynamical study described in Section 5.2.

Much of our data analysis was done using the PYNBODY software suite (Pontzen et al. 2013). Resources supporting this work were provided by the NASA High-End Computing (HEC) Program through the NASA Advanced Supercomputing (NAS) Division at Ames Research Centre. This research was conducted on Munsee Lenape land.

## DATA AVAILABILITY

The simulations analysed in this work (DC Justice League and MARVEL-ous Dwarfs) are proprietary and are not available to the public. The authors are happy to share quantitative data related to our results for collaborative purposes upon request.

## REFERENCES

- Akins H. B., Christensen C. R., Brooks A. M., Munshi F., Applebaum E., Engelhardt A., Chamberland L., 2021, *ApJ*, 909, 139
- Anderson L., Governato F., Karcher M., Quinn T., Wadsley J., 2017, *MNRAS*, 468, 4077
- Applebaum E., Brooks A. M., Quinn T. R., Christensen C. R., 2020, *MNRAS*, 492, 8
- Armitage P. J., Natarajan P., 2002, *ApJ*, 567, L9
- Baldassare V. F., Reines A. E., Gallo E., Greene J. E., 2017, *ApJ*, 850, 196
- Baldassare V. F., Geha M., Greene J., 2018, *ApJ*, 868, 152
- Baldassare V. F., Dickey C., Geha M., Reines A. E., 2020, *ApJ*, 898, L3
- Banik U., van den Bosch F. C., Tremmel M., More A., Despali G., More S., Vegetti S., McKean J. P., 2019, *MNRAS*, 483, 1558
- Begelman M. C., Volonteri M., Rees M. J., 2006, *MNRAS*, 370, 289
- Bellovary J. M., Cleary C. E., Munshi F., Tremmel M., Christensen C. R., Brooks A., Quinn T. R., 2019, *MNRAS*, 482, 2913
- Binney J., Mamon G. A., 1982, *MNRAS*, 200, 361
- Binney J., Tremaine S., 2008, *Galactic Dynamics*, 2nd edn. Princeton Univ. Press, Princeton, NJ
- Birchall K. L., Watson M. G., Aird J., 2020, *MNRAS*, 492, 2268
- Blecha L., Cox T. J., Loeb A., Hernquist L., 2011, *MNRAS*, 412, 2154
- Böker T., 2010, in de Grijs R., Lépine J. R. D., eds, *Star Clusters: Basic Galactic Building Blocks Throughout Time and Space*. Vol. 266 Proceedings of the International Astronomical Union, IAU Symposium. p. 58
- Boldrini P., Mohayaee R., Silk J., 2020, *MNRAS*, 495, L12
- Bryan G. L., Norman M. L., 1998, *ApJ*, 495, 80
- Cann J. M. et al., 2020, *ApJ*, 895, 147
- Chandrasekhar S., 1943, *ApJ*, 97, 255
- Chilingarian I. V., Katkov I. Y., Zolotukhin I. Y., Grishin K. A., Beletsky Y., Boutsia K., Osip D. J., 2018, *ApJ*, 863, 1
- Christensen C., Quinn T., Governato F., Stilp A., Shen S., Wadsley J., 2012, *MNRAS*, 425, 3058
- Colpi M., 2014, *Space Sci. Rev.*, 183, 189
- Dickey C. M., Geha M., Wetzel A., El-Badry K., 2019, *ApJ*, 884, 180
- EPA Carbon Offset Calculator, 2020, Available at: <https://www.epa.gov/energy/greenhouse-gases-equivalencies-calculator-calculations-and-references>
- Farrell S. A., Webb N. A., Barret D., Godet O., Rodrigues J. M., 2009, *Nature*, 460, 73
- Gill S. P. D., Knebe A., Gibson B. K., 2004, *MNRAS*, 351, 399
- Girardi L. et al., 2010, *ApJ*, 724, 1030
- Governato F. et al., 2012, *MNRAS*, 422, 1231
- Graham A. W., Scott N., 2015, *ApJ*, 798, 54
- Greene J. E., 2012, *Nat. Commun.*, 3, 1304
- Greene J. E., Strader J., Ho L. C., 2020, *ARA&A*, 58, 257
- Haardt F., Madau P., 2012, *ApJ*, 746, 125
- Haiman Z., Kocsis B., Menou K., 2009, *ApJ*, 700, 1952
- Holley-Bockelmann K., Khan F. M., 2015, *ApJ*, 810, 139
- Katz N., White S. D. M., 1993, *ApJ*, 412, 455
- Knollmann S. R., Knebe A., 2009, *ApJS*, 182, 608
- Kroupa P., 2001, *MNRAS*, 322, 231
- Lasota J. P., Alexander T., Dubus G., Barret D., Farrell S. A., Gehrels N., Godet O., Webb N. A., 2011, *ApJ*, 735, 89
- Lazar A. et al., 2020, *MNRAS*, 497, 2393
- Lodato G., Natarajan P., 2006, *MNRAS*, 371, 1813
- Ma L., Hopkins P. F., Ma X., Anglés-Alcázar D., Faucher-Giguère C.-A., Kelley L. Z., 2021, preprint ([arXiv:2101.02727](https://arxiv.org/abs/2101.02727))
- Marigo P., Girardi L., Bressan A., Groenewegen M. A. T., Silva L., Granato G. L., 2008, *A&A*, 482, 883
- Martínez-Palomera J., Lira P., Bhalla-Ladd I., Förster F., Plotkin R. M., 2020, *ApJ*, 889, 113
- Menon H., Wesolowski L., Zheng G., Jetley P., Kale L., Quinn T., Governato F., 2015, *Comput. Astrophys. Cosmol.*, 2, 1
- Mezcuca M., 2017, *Int. J. Modern Phys. D*, 26, 1730021
- Mezcuca M., Domínguez Sánchez H., 2020, *ApJ*, 898, L30
- Mezcuca M., Civano F., Marchesi S., Suh H., Fabbiano G., Volonteri M., 2018, *MNRAS*, 478, 2576
- Mezcuca M., Suh H., Civano F., 2019, *MNRAS*, 488, 685
- Miller B. P., Gallo E., Greene J. E., Kelly B. C., Treu T., Woo J.-H., Baldassare V., 2015, *ApJ*, 799, 98
- Moore B., 1994, *Nature*, 370, 629
- Moran E. C., Shahinyan K., Sugarman H. R., Vélez D. O., Eracleous M., 2014, *AJ*, 148, 136
- Munshi F. et al., 2013, *ApJ*, 766, 56
- Munshi F., Brooks A. M., Applebaum E., Weisz D. R., Governato F., Quinn T. R., 2017, preprint ([arXiv:1705.06286](https://arxiv.org/abs/1705.06286))
- Munshi F., Brooks A., Applebaum E., Christensen C., Sligh J. P., Quinn T., 2021, preprint ([arXiv:2101.05822](https://arxiv.org/abs/2101.05822))
- Oh S. P., Haiman Z., 2002, *ApJ*, 569, 558
- Pardo K. et al., 2016, *ApJ*, 831, 203
- Paynter J., Webster R., Thrane E., 2021, *Nat. Astron.*, Available at: <https://ui.adsabs.harvard.edu/abs/2021NatAs.tmp...55P/abstract>
- Planck Collaboration I., 2014, *A&A*, 571, A1
- Pontzen A., Roškar R., Stinson G. S., Woods R., Reed D. M., Coles J., Quinn T. R., 2013, pynbody: Astrophysics Simulation Analysis for Python
- Reines A. E., Greene J. E., Geha M., 2013, *ApJ*, 775, 116
- Reines A. E., Condon J. J., Darling J., Greene J. E., 2020, *ApJ*, 888, 36
- Relatores N. C. et al., 2019, *ApJ*, 887, 94
- Ricarte A., Natarajan P., 2018, *MNRAS*, 481, 3278
- Ritchie B. W., Thomas P. A., 2001, *MNRAS*, 323, 743
- Sanchez N. N., Werk J. K., Tremmel M., Pontzen A., Christensen C., Quinn T., Cruz A., 2019, *ApJ*, 882, 8
- Satyapal S., Secret N. J., McAlpine W., Ellison S. L., Fischer J., Rosenberg J. L., 2014, *ApJ*, 784, 113
- Sharma R. S., Brooks A. M., Somerville R. S., Tremmel M., Bellovary J., Wright A. C., Quinn T. R., 2020, *ApJ*, 897, 103
- Shen S., Wadsley J., Stinson G., 2010, *MNRAS*, 407, 1581
- Spaans M., Silk J., 2006, *ApJ*, 652, 902
- Spergel D. N. et al., 2007, *ApJS*, 170, 377
- Stadel J. G., 2001, PhD thesis, University of Washington
- Stevens A. R. H., Bellstedt S., Elahi P. J., Murphy M. T., 2020, *Nat. Astron.*, 4, 843
- Stinson G., Seth A., Katz N., Wadsley J., Governato F., Quinn T., 2006, *MNRAS*, 373, 1074
- Stinson G. S., Dalcanton J. J., Quinn T., Kaufmann T., Wadsley J., 2007, *ApJ*, 667, 170
- Top 500, 2020, Available at: <https://www.top500.org/system/177259/>
- Tremmel M., Governato F., Volonteri M., Quinn T. R., 2015, *MNRAS*, 451, 1868
- Tremmel M., Karcher M., Governato F., Volonteri M., Quinn T. R., Pontzen A., Anderson L., Bellovary J., 2017, *MNRAS*, 470, 1121
- Tremmel M., Governato F., Volonteri M., Pontzen A., Quinn T. R., 2018, *ApJ*, 857, L22
- True Valumetrics, 2020, Available at: <http://www.truevaluemetrics.org/DBpdfs/Forests/Tree-Nation-Tropical-tree-sequestration-of-CO2.pdf>



- van der Marel R. P., 1994, *MNRAS*, 270, 271  
 van der Marel R. P., Kallivayalil N., 2014, *ApJ*, 781, 121  
 Volonteri M., Natarajan P., 2009, *MNRAS*, 400, 1911  
 Wadsley J. W., Stadel J., Quinn T., 2004, *New Astron.*, 9, 137  
 Wadsley J. W., Keller B. W., Quinn T. R., 2017, *MNRAS*, 471, 2357  
 Wright A. C., Tremmel M., Brooks A. M., Munshi F., Nagai D., Sharma R. S., Quinn T. R., 2021, *MNRAS*, 502, 5370  
 Zaw I., Rosenthal M. J., Katkov I. Y., Gelfand J. D., Chen Y.-P., Greenhill L. J., Briske W., Noori H. A., 2020, *ApJ*, 897, 111

## APPENDIX A: CARBON FOOTPRINT CALCULATION

In order to raise awareness of the substantial impact of high-performance computing (HPC) to climate change, we calculate the carbon footprint of the eight simulations described in this work (four DC Justice League and four MARVEL-ous Dwarfs; we do not include the isolated galaxies described in Section 5.2 because this footprint is orders of magnitude smaller). We are inspired by the recent work by Stevens et al. (2020), who estimate that among Australian astronomers the carbon footprint of supercomputer use is greater than all other carbon-emitting sources *combined*, and is larger than the next-lowest source (travel) by a factor of 4.

The carbon emissions related to a simulation’s production depend on several factors, including the power  $P_{\text{HPC}}$  used by the computer (itself dependent on the number of cores  $n_{\text{cores}}$  used) and the run time of the simulation  $t_{\text{sim}}$ . Each of our simulations used slightly different numbers of cores and ran for varying amounts of time; for the sake of simplicity, we do this calculation in an order-of-magnitude fashion.

The Justice League and MARVEL simulations were run on the Pleiades supercomputer located at NASA Ames Research Centre.

The website Top500.org lists the environmental impact of the worlds’ leading HPC centres, including information such as power consumption and total number of cores. Using data from 2017 June (a month when several of our simulations were running), the NASA HEC Centre self-reports a power consumption of 4407 kW, and hosts 241 108 cores (Top 500 2020) for Pleiades. Assuming equal power consumption across cores, and using the base value of  $n_{\text{cores}} = 1000$  for each our simulations, we calculate the total power consumption of one simulation to be  $P_{\text{HPC}} = 18.27$  kW.

Each simulation takes a total of 3–6 months to run on average, but this total includes queue wait times, where no computation occurs. We use our average value of  $t_{\text{sim}} = 94$  d of time for computation. The total energy expended for one simulation is thus  $P_{\text{HPC}} \times t_{\text{sim}} = 412\,354$  kWh for one simulation, or 3298 834 kWh for all eight.

We convert energy to amount of  $\text{CO}_2$  using the EPA’s calculations for home energy use (EPA Carbon Offset Calculator 2020), which assumes an output of 0.454 kg  $\text{CO}_2$  per kWh of energy. The total amount of carbon dioxide we have expelled into the Earth’s atmosphere with our simulations equals 1497 670 kg of  $\text{CO}_2$ .

While there are many ways to offset carbon emissions, a straightforward one is to simply plant trees. Assuming a typical tree absorbs 158 kg of  $\text{CO}_2$  in a year (True Valumetrics 2020), and lives for 20 yr, we calculate that our collaboration should plant 474 trees. The cost of trees varies greatly by geographic location and species, but is rarely prohibitive. We encourage researchers to include tree-planting or equivalent carbon offsets in funding proposals.

This paper has been typeset from a  $\text{\LaTeX}$  file prepared by the author.